

Excitatory and inhibitory receptors utilize distinct post- and trans-synaptic mechanisms in vivo

Taisuke Miyazaki^{1,2,3}, Megumi Morimoto-Tomita¹, Coralie Berthoux⁴, Kotaro Konno³, Yoav Noam¹, Tokiwa Yamasaki¹, Matthijs Verhage⁵, Pablo E Castillo⁴, Masahiko Watanabe³, Susumu Tomita^{1*}

¹Department of Cellular and Molecular Physiology, Department of Neuroscience, Yale University School of Medicine, New Haven, United States; ²Department of Health Sciences, School of Medicine, Hokkaido University, Sapporo, Japan; ³Department of Anatomy, Faculty of Medicine, Hokkaido University, Sapporo, Japan; ⁴Dominick P. Purpura Department of Neuroscience, Albert Einstein College of Medicine, Bronx, United States; ⁵Department of Clinical Genetics, Center for Neurogenomics and Cognitive Research (CNCR), VU University Amsterdam and VU Medical Center, Amsterdam, Netherlands

Abstract Ionotropic neurotransmitter receptors at postsynapses mediate fast synaptic transmission upon binding of the neurotransmitter. Post- and trans-synaptic mechanisms through cytosolic, membrane, and secreted proteins have been proposed to localize neurotransmitter receptors at postsynapses. However, it remains unknown which mechanism is crucial to maintain neurotransmitter receptors at postsynapses. In this study, we ablated excitatory or inhibitory neurons in adult mouse brains in a cell-autonomous manner. Unexpectedly, we found that excitatory AMPA receptors remain at the postsynaptic density upon ablation of excitatory presynaptic terminals. In contrast, inhibitory GABA_A receptors required inhibitory presynaptic terminals for their postsynaptic localization. Consistent with this finding, ectopic expression at excitatory presynapses of neurexin-3 alpha, a putative trans-synaptic interactor with the native GABA_A receptor complex, could recruit GABA_A receptors to contacted postsynaptic sites. These results establish distinct mechanisms for the maintenance of excitatory and inhibitory postsynaptic receptors in the mature mammalian brain.

*For correspondence:
susumu.tomita@yale.edu

Competing interest: The authors declare that no competing interests exist.

Funding: See page 18

Received: 03 June 2020

Accepted: 19 September 2021

Published: 18 October 2021

Reviewing Editor: Eunjoon Kim, Institute for Basic Science, Korea Advanced Institute of Science and Technology, Republic of Korea

© Copyright Miyazaki et al. This article is distributed under the terms of the [Creative Commons Attribution License](https://creativecommons.org/licenses/by/4.0/), which permits unrestricted use and redistribution provided that the original author and source are credited.

Introduction

Fast excitatory and inhibitory synaptic transmissions in the mature brain are mostly mediated by ionotropic AMPA-type glutamate receptors (AMPA_Rs) and GABA_A receptors (GABA_AR_s), respectively. The maintenance of these receptors at the corresponding postsynapse involves various components, including postsynaptic cytosolic scaffolding proteins and trans-synaptic components, such as membrane and secreted proteins (*Barrera-Ocampo and Chater, 2013; Gerrow and El-Husseini, 2007; Luscher et al., 2011; Martenson and Tomita, 2015; Moss and Smart, 2001*). However, it is less clear which of these mechanisms is crucial for maintaining neurotransmitter receptors at postsynapses in vivo.

Acetylcholine receptors remain at synapses of the neuromuscular junction after denervation, highlighting the importance of the postsynaptic machinery for its maintenance at synapses (*Hartzell and Fambrough, 1972*). As denervation of specific neurons is not feasible in the brain, alternative approaches such as X-irradiation have been attempted to induce neuronal loss, for example, in the cerebellum (*Altman and Anderson, 1972; Bayer and Altman, 1975*). The specificity of the neuronal

loss was later improved with genetic and pharmacological approaches, such as by expression of a toxin gene or exogenous receptor/enzyme expression combined with agonist administration (Gray et al., 2010; Palmiter et al., 1987; Watanabe et al., 1998; Yang et al., 2013). To date, these methods have been limited in their ability to uncover mechanisms of postsynaptic receptor localization mainly due to pleiotropic effects.

Loss of Syntaxin-binding protein 1 (Stxbp1 – also known as Munc18-1) results in massive neurodegeneration (Verhage et al., 2000), and expression of Cre recombinase in primary cultured neurons from conditional Stxbp1 homozygous mice (*Stxbp1^{fl/fl}*) induces neuronal death in a cell-autonomous manner (Heeroma et al., 2004). Moreover, Cre recombinase expression under *Pcp2* and *Sert* promoters results in degeneration of cerebellar Purkinje cells (PCs) and serotonin (5-HT) neurons, respectively (Dudok et al., 2011; Heeroma et al., 2004). Here, we took advantage of the cell-autonomous elimination observed in Stxbp1 homozygous neurons (Dudok et al., 2011; Heeroma et al., 2004) to investigate the machinery responsible for maintaining neurotransmitter receptors at postsynapses.

Results

Selective removal of granule cells and PCs in the mature brain

The cerebellum consists of the molecular layer (ML), the Purkinje cell layer (PCL), the granular layer (GL), and deep cerebellar nuclei (DCN) in the white matter (Figure 1A). Granule cells (GCs) in the GL form excitatory glutamatergic synapses with PCs and molecular layer interneurons (MLIs) in the ML. MLIs form inhibitory GABAergic synapses with PCs, which then form inhibitory synapses with DCN (Figure 1A). We took advantage of the well-defined neuronal and synaptic organization of the cerebellum to investigate the roles of presynaptic components in maintaining excitatory or inhibitory receptors.

We crossed conditional Stxbp1 mice (*Stxbp1^{fl/fl}*) with transgenic mouse lines expressing Cre recombinase under the *Gabra6* promoter for GCs (Fünfschilling and Reichardt, 2002) or the *Pcp2* promoter for PCs (Barski et al., 2000), and obtained *Gabra6-Cre: Stxbp1^{fl/fl}* (Δ GC) and *Pcp2-Cre: Stxbp1^{fl/fl}* (Δ PC) mice. We used littermates that did not carry a transgene of Cre recombinase (control) for comparison. Δ GC and Δ PC mice began to show obvious locomotor phenotypes at around P28 (Figure 1B and Videos 1 and 2).

Nissl staining demonstrated the loss of GCs in Δ GC mice and PCs in Δ PC mice at 2 months of age (Figure 1C), but no obvious differences at postnatal days 7–9 (P7–9) (Figure 1—figure supplement 1). The total area of midsagittal cerebellar sections was significantly smaller in Δ GC and Δ PC mice than in control mice (Figure 1C and D). In Δ GC mice, the thickness of the GL was reduced by 82%, but the PCL was intact. By contrast, the PCL disappeared with no change of the GL thickness in Δ PC mice. We also found a significant reduction in the ML thickness in both mice: 43.4% and 24.9% reduction in Δ GC and Δ PC mice, respectively (Figure 1D). The degrees of reduction are comparable to volume fraction of parallel fiber (PF) (Napper and Harvey, 1988) and PC dendrites (Hamodeh et al., 2010; Roth and Häusser, 2001). These results indicate that GCs and PCs were selectively and effectively eliminated in a cell-autonomous manner from the adult Δ GC and Δ PC cerebella.

Excitatory receptors remain at postsynapses upon presynaptic ablation

We examined whether presynaptic components are required to maintain excitatory receptors by analyzing receptor localization on presynapse-free postsynapses. GCs project PFs to form excitatory glutamatergic synapses onto PC spines and MLI dendritic shafts (Figure 1A). In adult Δ GC mice, PF ablation was confirmed by loss of the PF protein vesicular glutamate transporter (VGLUT1) (Miyazaki et al., 2003) in the ML, except the very surface of the ML and thinned GL (Figure 2A). These results indicate that excitatory PF inputs to PCs and MLIs are mostly ablated in adult Δ GC mice.

Given that orphan GluD2 receptors selectively localize at PF–PC postsynapses (Landsend et al., 1997), we utilized GluD2 as a marker of PF–PC postsynapses. Punctate signals of GluD2 were observed in both control and Δ GC mice with a 26 % increase of signal intensity in Δ GC mice (Figure 2B), which is presumably due to condensation of GluD2 puncta in a thinned ML (Figure 1C). Notably, GluD2 signal was stronger at the surface of the ML (Figure 2B), where VGLUT1-labeled PFs remained (Figure 2A). In electron microscopy analysis (Figure 2C), all PC spines were contacted and formed asymmetrical synapses in the control mice (contacted spine), whereas most spines in the

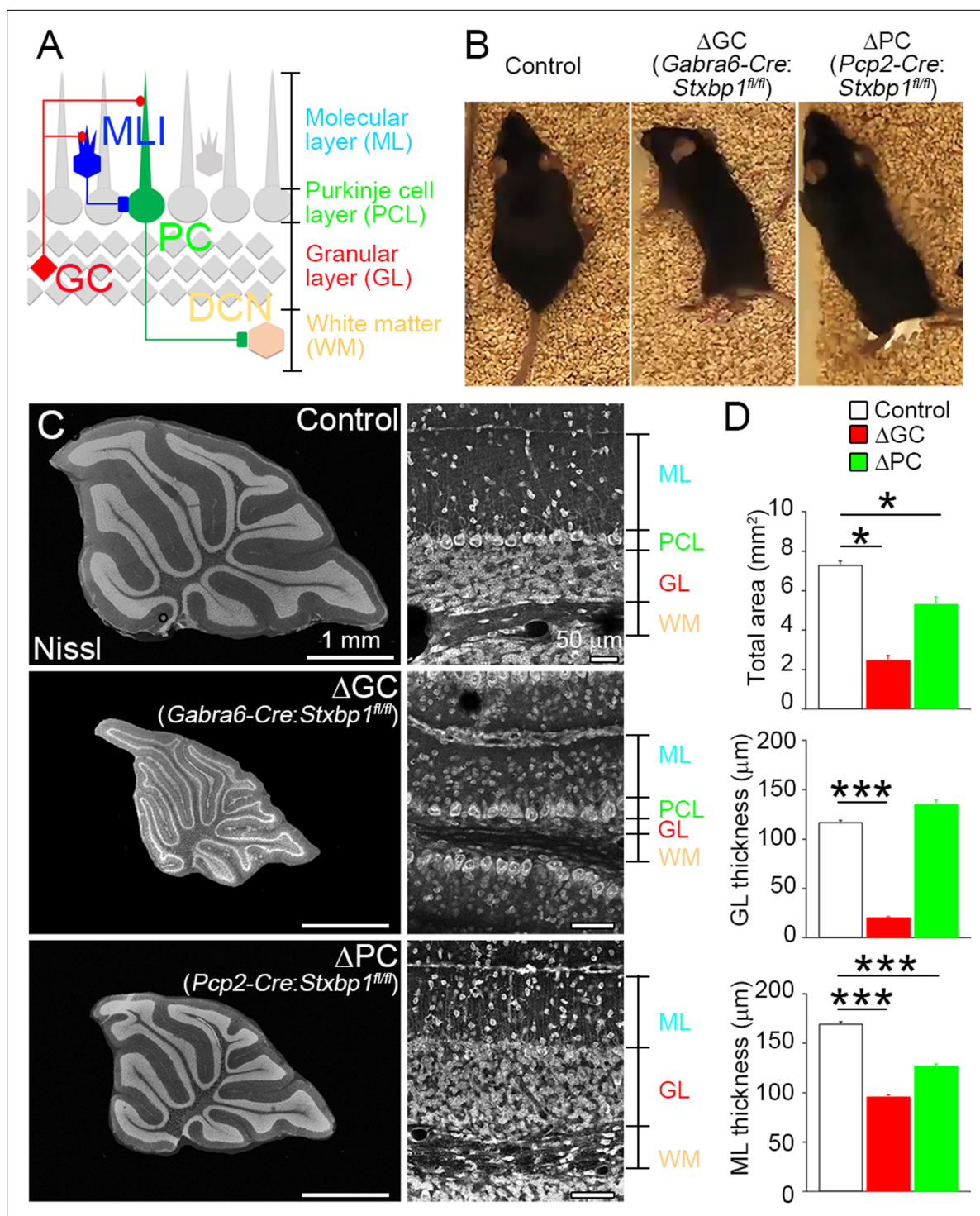


Figure 1. Adult cerebellar organization after cell-autonomous elimination of neurons. **(A)** Synaptic circuit organization in the adult cerebellum. Granule cells (GCs) send excitatory inputs to Purkinje cells (PCs) and molecular layer interneurons (MLIs). MLIs form inhibitory synapses on to PCs that send inhibitory inputs to the deep cerebellar nucleus (DCN). **(B)** Cerebellar GC- and PC-specific conditional *Stxbp1* homozygous mice (Δ GC mice and Δ PC mice, respectively) manifest ataxia at 5–6 months of age (see Extended Data **Videos 1 and 2**). **(C)** Cerebellar histology of control (top), Δ GC (middle), and Δ PC (bottom) mice at P30. **(D)** Significant decrease in the total cerebellar area and the thicknesses of granular layer (GL) and molecular layer (ML) (n = 45–67 regions from three mice each). Note that gross histoarchitecture of cerebellum is maintained in Δ GC and Δ PC mice. Data are means \pm SEMs; Kruskal–Wallis test with Steel post-test; *p < 0.05, ***p < 0.001. The numerical values are summarized in source data.

The online version of this article includes the following source data and figure supplement(s) for figure 1:

Figure 1 continued on next page

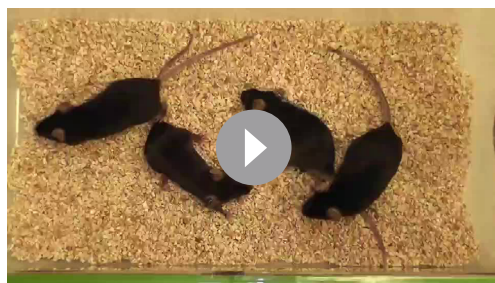
Figure 1 continued

Source data 1. Adult cerebellar organization after cell-autonomous elimination of neurons.**Figure supplement 1.** Normal cerebellar histology of mouse brains at P7–9.

Δ GC mice ($87.1\% \pm 1.5\%$) were free of innervation (free spine) and wrapped by Bergmann glia (BG in **Figure 2C**). Surprisingly, no difference was observed in the spine number between control and Δ GC mice (control, 0.45 ± 0.03 and Δ GC, 0.42 ± 0.02 spines per μm of PC dendrite, $n = 142$ from three mice each). Moreover, thick postsynaptic density (PSD), which is typical of asymmetrical synapses, was also discerned on free spines. The immunogold AMPAR particle density in dendritic spines colabeled with PC protein Car8 was similar between contacted spines in control mice and free spines in Δ GC mice (**Figure 2D**).

We next examined whether AMPARs at free spines were functional by performing two-photon uncaging of glutamate on individual dendritic spines in acute sagittal cerebellar slices perfused with MNI-glutamate (**Figure 2E**). Dendritic spines were identified by loading PCs with Alexa 594 (**Figure 2F**). We found that uncaging glutamate-evoked excitatory postsynaptic currents were undistinguishable in control and Δ GC mice (control, 32 ± 3.9 pA, $n = 6$ from three mice; Δ GC, 30 ± 3.9 pA, $n = 7$ from four mice; $p = 0.8037$, unpaired t-test), and these responses were abolished by the AMPAR antagonist NBQX (**Figure 2G and H**). These results indicate that postsynaptic structure and AMPAR localization at the PSD are maintained on PC spines in the absence of presynaptic terminals (**Figure 2I**).

Unlike spiny PF–PC synapses, PF–MLI synapses are established on the dendritic shaft. In immunostaining for PSD-95, which accumulates at the MLI postsynapse (**Fukaya and Watanabe, 2000**), Δ GC mice exhibited a 46 % reduction in the density of, and a 43 % increase in the size of individual PSD-95 puncta (**Figure 3A**). Electron microscopy showed that all PSDs were observed on the postsynaptic side of axodendritic shaft PF–MLI synapses in control mice (**Figure 3B, left**), while in Δ GC mice the vast majority ($85.8\% \pm 2.2\%$, $n = 6$ images from three mice each) was found in both sides of atypical dendrodendritic contacts between MLIs (**Figure 3B, right**). At this unique contact site, we did not observe accumulation of synaptic vesicles with around 40 nm in diameter (**Figure 3B**). The cleft width of the dendrodendritic contact in Δ GC mice (30.0 ± 1.0 nm) was wider than that of axodendritic synapse in control mice (15.8 ± 0.5 nm, $n = 63\text{--}73$ from three mice each). Notably, while AMPARs were localized only on the postsynaptic side in control mice, they were detected on both sides of dendrodendritic contacts and exhibited a twofold increase in Δ GC mice (**Figure 3C**). Furthermore, presynaptic active zone protein bassoon, which was localized at the PF–MLI synapses in control mice (**Figure 3D and E, left**), disappeared from dendrodendritic contact in Δ GC mice (right). We also confirmed the lack of VGluT1 labeling at around dendrodendritic contact (**Figure 3F**). These results suggest that the loss of presynaptic elements in vivo induces homophilic interaction between excitatory postsynapses on neighboring MLIs and transforms PF–MLI synapse into unique dendrodendritic contact, at which AMPARs continue to localize at the PSD-like specialization, but presynaptic molecules are no longer clustered (**Figure 3G**). Therefore, after presynaptic neuron ablation, AMPAR clustering is maintained at two distinct types of excitatory synapses, both being at the PSD-like specialization on dendritic spines of PCs and on dendritic shafts of MLIs.



Video 1. Sample video of two mice eliminating cerebellar granule cells (Δ GC) and two control mice.
<https://elifesciences.org/articles/59613/figures#video1>



Video 2. Sample video of two mice eliminating cerebellar Purkinje cells (Δ PC) and two control mice.
<https://elifesciences.org/articles/59613/figures#video2>

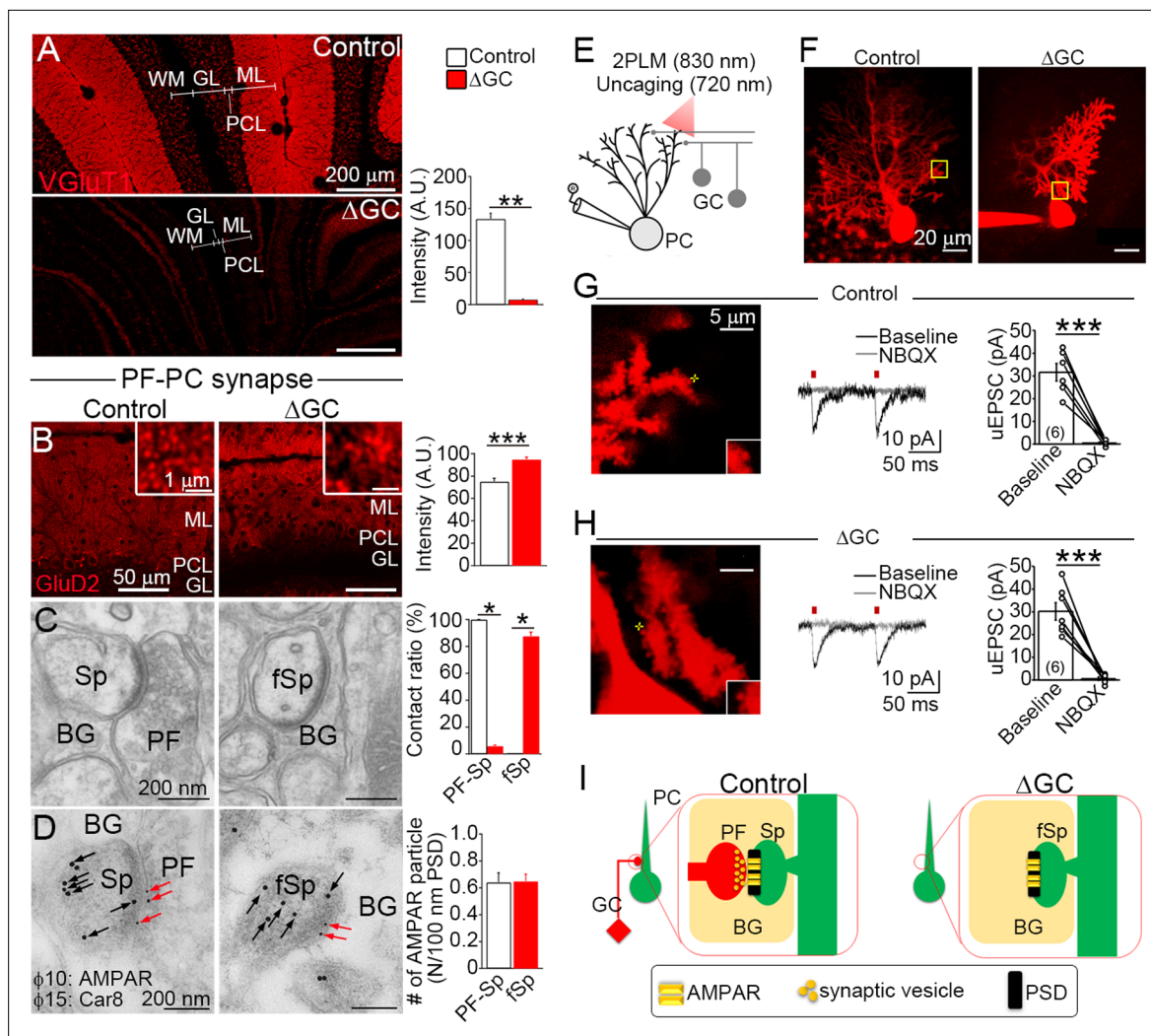


Figure 2. Excitatory AMPARs remain at spiny synapses without presynaptic terminals. **(A)** Vesicular glutamate transporter (VGLUT1) signal from GC axons, that is, parallel fibers (PFs), is significantly decreased in the molecular layer (ML) of the Δ GC mice ($n = 6$ images from three mice each). A.U.: arbitrary units. **(B–D)** Analysis of parallel fiber (PF)–Purkinje cell (PC) spiny synapses. **(B)** GluD2 show punctate localization in the ML and increase signal intensity in the Δ GC mice ($n = 20$ images from three mice each). A.U.: arbitrary units. **(C)** Electron micrographs showing a spine (Sp) making synaptic contact with a PF in a control mouse and a free spine (fSp) lacking synaptic contact in a Δ GC mouse ($n = 6$ regions from three mice each). BG: Bergmann glia. **(D)** Postembedding immunogold for panAMPA (10 nm, red arrows) on Car8 (15 nm, black arrows)-labeled PC spines (Sp) or a free spine (fSp) in control and Δ GC mice, respectively ($n = 114$ – 130 from three mice each). BG: Bergmann glia. **(E)** Schematic diagram illustrating the experimental design of combined electrophysiology, imaging and uncaging in acute cerebellar slices from Δ GC and control littermates. Excitation wavelengths employed were 830 nm (for imaging) and 720 nm (for glutamate uncaging). **(F)** 2 P reconstruction of a Purkinje cells loaded with Alexa 594 in Δ GC and control mice. Left, example of the position of the uncaging laser beam (yellow cross) in control **(G)** and Δ GC **(H)** littermates. Middle, representative uncaging glutamate-evoked excitatory postsynaptic currents (uEPSCs). NBQX (10 μ M) was bath applied to block AMPARs. Right, summary plot demonstrating that NBQX (10 μ M) inhibits uEPSC evoked by glutamate uncaging (control, 6 cells from 3 mice; Δ GC, 7 cells from 4 mice). Data are presented as mean \pm SEM. *** $p < 0.001$, paired t -test. **(I)** After ablation of PFs AMPAR clustering and postsynaptic density (PSD)-like specialization are maintained on free PC spines in Δ GC mice. BG: Bergmann glia. Data are means \pm SEMs, Mann–Whitney U -test **(A–D)**, * $p < 0.05$, ** $p < 0.01$, *** $p < 0.001$. The numerical values are summarized in source data.

The online version of this article includes the following source data for figure 2:

Source data 1. Excitatory AMPARs remain at spiny synapses without presynaptic terminals.

Inhibitory postsynaptic receptor localization requires presynaptic components

We next evaluated the role of presynaptic components in maintaining inhibitory receptors at GABAergic PC–DCN synapses (**Figure 1A**). In Δ PC mice, calbindin-positive PC axon terminals and

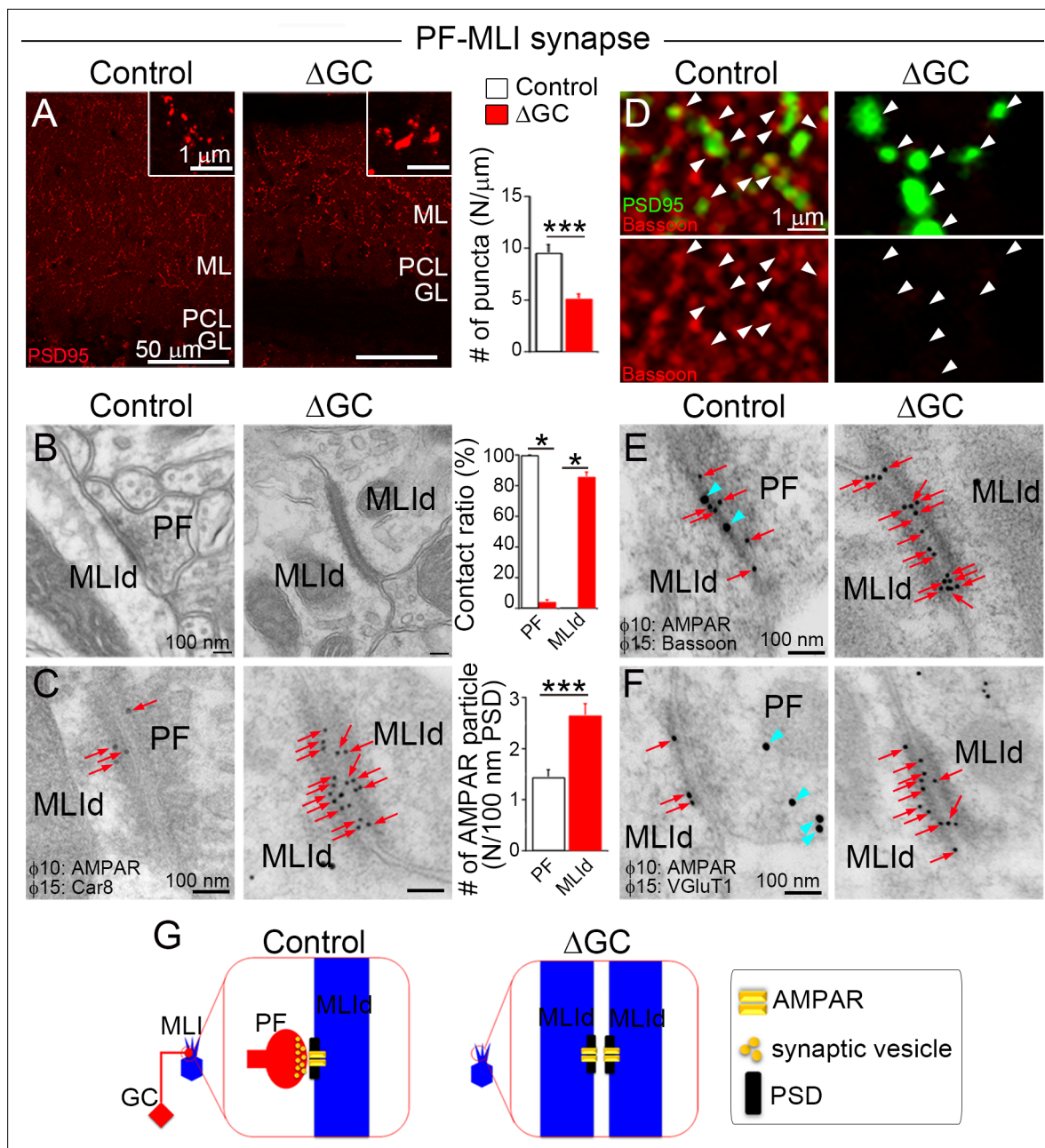


Figure 3. Excitatory AMPARs remain at shaft synapses without presynaptic terminals. **(A)** The number of postsynaptic density (PSD)-95 puncta is reduced ($n = 6$ images from three mice each) and individual puncta is enlarged in molecular layer (ML) of the Δ GC mice ($n = 1421$ puncta in control and 686 in Δ GC from three mice each). **(B)** Electron micrographs showing a typical parallel fiber (PF)–molecular layer interneuron (MLI) synapse on MLI dendritic shaft (MLId) shaft synapse in a control mouse and an atypical dendrodendritic contact between MLIs in a Δ GC mouse ($n = 6$ images from three mice each). **(C)** Postembedding immunogold for panAMPA (10 nm, red arrows) and Car8 (15 nm) ($n = 25$ –42 from three mice each). Dendrites of MLI are identified by negative labeling for Car8 and the lack of dendritic spines. A bar graph shows the contact ratio of MLId with PF terminals or other MLId. **(D)** Double immunofluorescence for bassoon (red) and PSD-95 (green). Arrowheads indicate PSD-positive puncta. Note that PSD-95 signals are facing to bassoon signals in control. **(E, F)** Double-labeling postembedding immunogold for panAMPA (10 nm, red arrows) ($n = 25$ –42 from three mice each) and active zone protein, bassoon (15 nm, blue arrowheads in E) or synaptic vesicle-associated protein vesicular glutamate transporter (VGluT1) (15 nm, blue arrowheads in F). Presynaptic proteins bassoon and VGluT1 are not detected at and around dendrodendritic contact sites. **(G)** After ablation of PFs, AMPAR clustering and PSD-like specialization are maintained in dendrodendritic contact sites between MLIs in Δ GC mice. Data are means \pm SEMs, Mann–Whitney U -test (**A–C**), * $p < 0.05$, *** $p < 0.001$. The numerical values are summarized in source data.

The online version of this article includes the following source data for figure 3:

Source data 1. Excitatory AMPARs remain at shaft synapses without presynaptic terminals.

vesicular inhibitory amino acid transporter (VIAAT)-positive inhibitory terminals were substantially reduced in the DCN (**Figure 4A**). A few VIAAT clusters remained in the DCN of Δ PC mice, which likely originate from local inhibitory DCN neurons (*Uusisaari and Knöpfel, 2011*), residual 18.9 % PCs, or both.

In control mice, the GABA_AR α 1 subunit was clustered on somatic membranes of DCN neurons just underneath VIAAT-positive terminals (**Figure 4B and C**). The number of GABA_AR α 1 puncta was significantly reduced in Δ PC mice (**Figure 4C and D**), corresponding to the reduction in VIAAT puncta (**Figure 4D**, bottom). On the DCN somata, the remaining GABA_AR α 1 signal was either dispersed weakly along the somatic membrane or accumulated intensely at sites just underneath remaining VIAAT puncta (**Figure 4C**). These results suggest presynaptic requirement for the maintenance of inhibitory GABA_AR clustering at PC–DCN synapses (**Figure 4E**).

To further investigate the role of presynaptic components in inhibitory receptor localization at GABAergic MLI–PC synapses, we adopted an adenoassociated virus (AAV)-based approach (**Figure 5A**), because of lethality of *Stxbp1^{fl/fl}* mice when crossed with Cre lines (*Nos1-Cre* and *PV-Cre*) for MLI ablation. As candidate promoters in AAV vectors expressing GFP (green fluorescent protein), we cloned 2 kb genomic fragments upstream of the TATA boxes from three genes, *Nos1*, *Grin3a*, and *Kit*, as they are explicitly expressed in adult MLIs according to the Allen Brain Atlas (<https://portal.brain-map.org/>). Among these constructs, we found that only the *Nos1* promoter showed GFP expression in MLIs locating at lower ML, but not in PCs (**Figure 5B and C**). Next, we introduced the *Nos1* promoter-driven Cre recombinase into *Stxbp1^{fl/fl}* cerebella. By immunostaining for parvalbumin (PV) and VIAAT, mice expressing *Nos1* promoter-driven Cre recombinase showed a significant reduction in neuronal elements of lower MLIs or basket cells (Δ MLI), that is, PV-labeled somata in the lower ML VIAAT-labeled presynaptic terminals around PC somata, and PV/VIAAT-labeled pinceau formation at the base of PC somata (**Figure 5D–F**). Importantly, GABA_AR α 1 clusters on PC somata were also reduced significantly in Δ MLI, especially at somatic surface devoid of contact with VIAAT-labeled presynaptic terminals (**Figure 5E–H**). Therefore, after presynaptic ablation, GABA_AR is declustered at two distinct inhibitory cerebellar synapses.

GABA_ARs can be recruited trans-synaptically to neighboring postsynaptic sites

Our results suggest that presynaptic components trans-synaptically control postsynaptic clustering of GABA_AR in vivo. If so, ectopic expression of presynaptic regulatory molecules could recruit GABA_ARs to apposed postsynaptic sites. We previously identified five components of the native GABA_AR complex, namely GABA_AR α , β , and γ subunits, GARLH3/4, and neuroligin-2 (*Yamasaki et al., 2017*). Knockdown or knockout of GARLH4/LHFPL4 results in a loss of synaptic GABA_AR clustering and inhibitory transmission, though GABA_ARs are retained on the neuronal surface (*Davenport et al., 2017; Wu et al., 2018; Yamasaki et al., 2017*), similar to what we observed in DCN neurons of Δ PC mice (**Figure 4C**). Neuroligin interacts with presynaptic neurexins (*Craig and Kang, 2007; Dean and Dresbach, 2006; Südhof, 2008*), which are necessary for excitatory or inhibitory transmission (*Chen et al., 2017*). However, it remains unknown whether ectopic neurexin expression at excitatory terminals can trans-synaptically recruit inhibitory GABA_ARs to postsynaptic sites in the brain.

We focused on neurexin-3 (*Nrxn3*) and excitatory climbing fiber (CF–PC synapses), because *Nrxn3* knockout specifically eliminates inhibitory transmission in the olfactory bulb (*Aoto et al., 2015*), and also because the inferior olivary nucleus (ION) projecting CFs are located distantly from PCs and this provides experimental advantage to avoid potential contamination of AAVs into PCs (**Figure 6A**). We first examined whether neurexin-3 alpha (*Nrxn3 α*) can interact with the GABA_AR/GARLH/NL complex. The extracellular domain of *Nrxn2 β* fused with the Fc domain of human immunoglobulin is shown to interact with GABA_ARs (*Zhang et al., 2010*). We purified the extracellular domain of mouse *Nrxn3 α* with splice site four fused with Fc and secreted Fc alone using transfected 293T cells (*Nrxn3 α* -Fc). We found that *Nrxn3 α* -Fc pulled down NL2, GABA_AR γ 2 subunits, and GARLH4, but not GluA1 AMPAR, from adult mouse cerebellar lysate, in a calcium-dependent manner (**Figure 6B**).

We next examined whether ectopically expressed *Nrxn3 α* in the excitatory CF terminal can recruit GABA_ARs at the contact site on PCs. We generated AAVs carrying either GFP or *Nrxn3 α* fused with GFP (*Nrxn3 α* -GFP) and injected them into the ION of wild-type mice at P21 (**Figure 6A**). One month after AAV injection, the GFP-positive varicosities were overlapped with CF presynaptic marker VGlut2

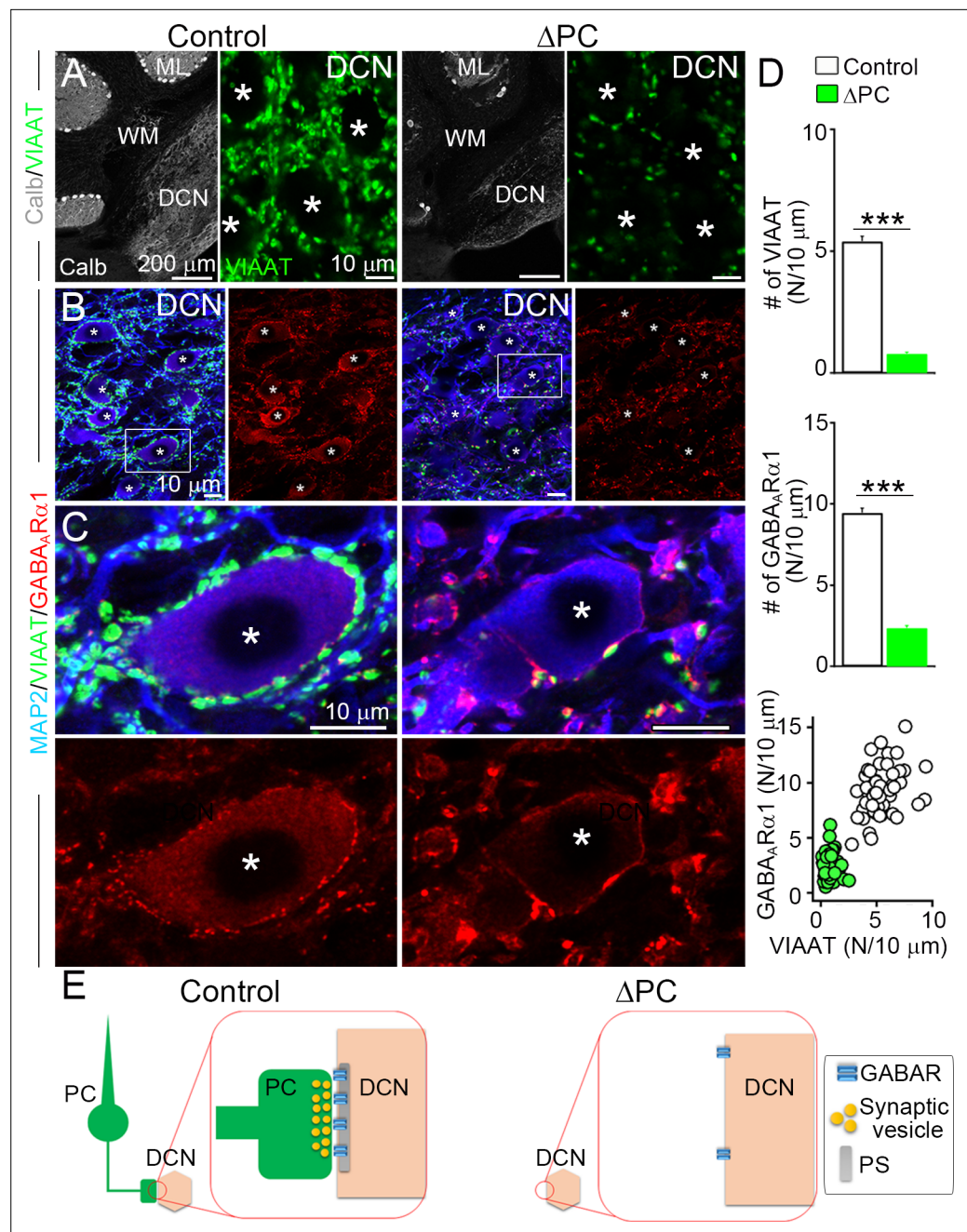


Figure 4. Inhibitory GABA_ARs require presynaptic terminals in the deep cerebellar nuclei (DCN). **(A)** Immunofluorescence showing marked reductions of calbindin (Calb)-labeled Purkinje cells (PCs) in the cerebellar cortex and of vesicular inhibitory amino acid transporter (VIAAT)-labeled inhibitory terminals in the DCN of the ΔPC mice. **(B, C)** Triple immunofluorescence for MAP2(microtubule associated protein 2) (blue), VIAAT (green), and GABA_ARα1 (red) in DCN boxed regions in B are enlarged in C. Asterisks indicate cell bodies of DCN neurons, which are fringed by numerous bright clusters of GABA_ARα1 in control mice but are greatly reduced in ΔPC mice. **(D)** Bar graphs showing reduced densities of VIAAT (top)- and GABA_ARα1 (middle)-positive puncta on the surface of DCN neurons in ΔPC mice (number per 10 μm, n = 49–60 neurons from three mice each). Kruskal–Wallis test followed by Steel–Dwass post-test for the comparison of scatter plot (bottom) indicates significant reduction (p < 0.001). **(E)** After ablation of PC terminals, postsynaptic GABA_ARα1 is declustered from somatic membrane of DCN neuron. Data are shown as means ± SEMs, ***p < 0.001. The numerical values are summarized in source data. The online version of this article includes the following source data for figure 4:

Source data 1. Inhibitory GABA_ARs require presynaptic terminals in the deep cerebellar nuclei (DCN).

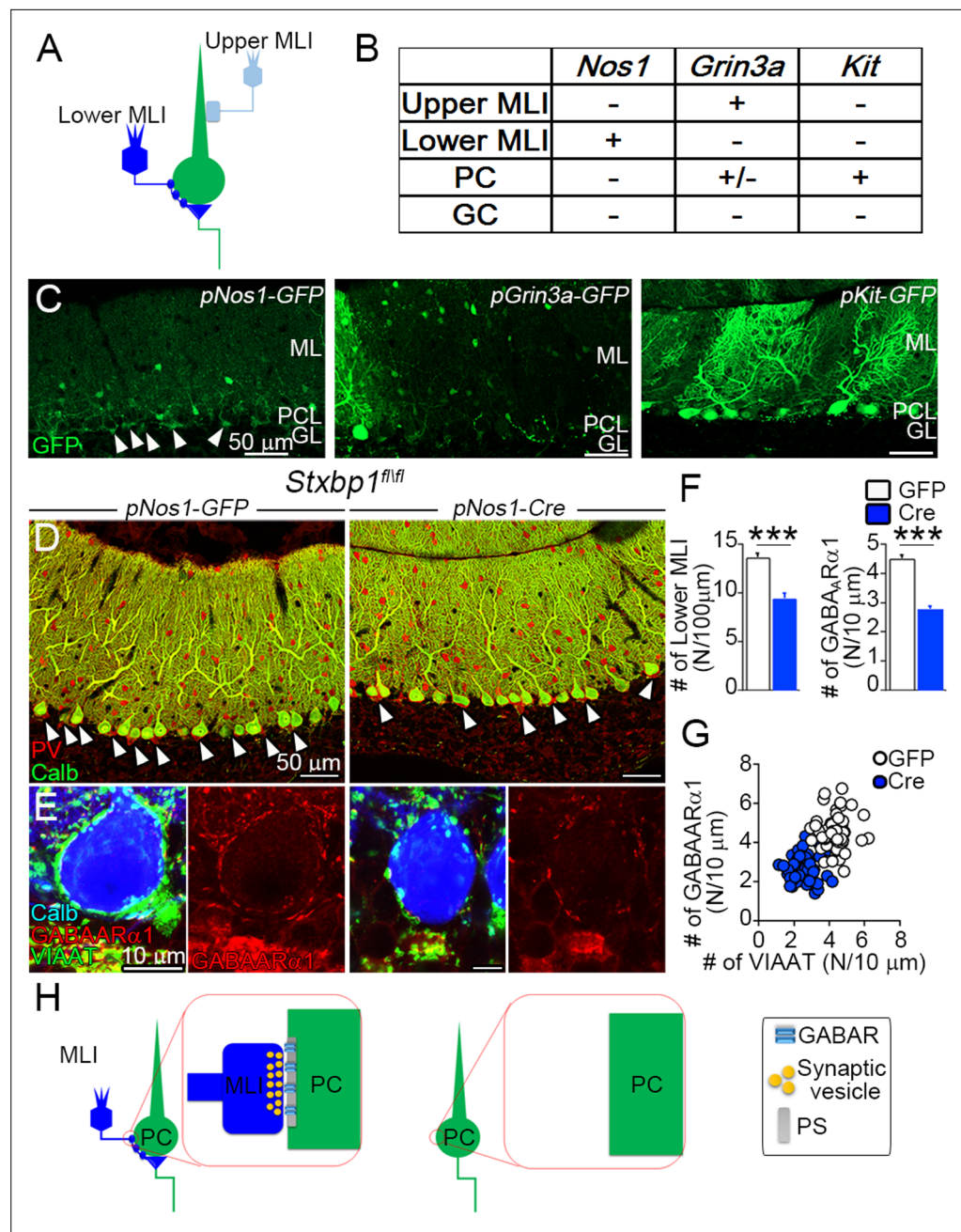


Figure 5. Inhibitory postsynaptic sites at Purkinje cell (PC) somas require presynaptic terminals. **(A)** Wiring diagram between molecular layer interneurons (MLIs) and PCs. Lower MLIs, also known as basket cells, innervate PC somata and surround the axon initial segment of PCs with the pinceau formation. Upper MLIs corresponding to stellate cells innervate dendritic shafts of PCs. **(B, C)** Adenoassociated viruses (AAVs) under different promoters targeting to MLIs. Summary of GFP expression is shown in a table **(B)** and representative images **(C)**. GFP expression is found preferentially in lower MLIs and pinceau formation in AAV pNos1-GFP (arrowheads in C). **(D, E)** Cerebella of *Stxbp1^{fl/fl}* mice-injected AAV pNos1-GFP (right) and -Cre (left). Multiple labeling for calbindin (green) and parvalbumin (red) in D and for GABA_AR α 1 (red), vesicular inhibitory amino acid transporter (VIAAT) (green), and calbindin (blue) in E. **(F)** The densities of lower MLIs (left, N/100 μ m of PC layer, $n = 12$ –15 images from three mice each, Mann–Whitney *U*-test) and GABA_AR α 1-positive puncta on PC somata (right, N/10 μ m of membrane, $n = 55$ neurons from three mice each, Student's *t*-test). **(G)** Scatter plot of the number of GABA_AR α 1- (vertical axis) against VIAAT-positive puncta (horizontal axis) on the surface of each PC soma (N/10 μ m, right, $n = 55$ neuron from 3 mice each, one-way analysis of variance) (ANOVA) ($F(3,216) = 94.8$, with Bonferroni post hoc test, $p < 0.001$). **(H)** Postsynaptic GABA_AR α 1 requires inhibitory presynaptic terminals at MLI–PC synapse. After ablation of MLI

Figure 5 continued on next page

Figure 5 continued

terminals, postsynaptic GABA_AR α 1 is declustered from somatic membrane of PC. Data are shown as means \pm SEMs; *** $p < 0.001$. The numerical values are summarized in source data.

The online version of this article includes the following source data for figure 5:

Source data 1. Inhibitory postsynaptic sites at Purkinje cell (PC) somas require presynaptic terminals.

and the numbers of GFP-positive varicosities were similar between mice expressing GFP and those expressing Nrnx3 α -GFP (**Figure 6C**). These results demonstrate successful introduction of GFP and Nrnx3 α -GFP into CFs without affecting target innervation. We next investigated the localization of the GABA_AR α 1 subunit, a major GABA_AR subunit in PCs (**Fritschy et al., 2006**) on PCs of AAV-injected mice. Some GABA_AR α 1-positive puncta overlapped with GFP or Nrnx3 α -GFP signals (**Figure 6D and E**). The area and number of varicosities with overlapping GFP and GABA_AR α 1 signals were significantly higher in animals injected with Nrnx3 α -GFP than in those receiving the vector with GFP alone (**Figure 6E**). These results indicate that ectopic expression of Nrnx3 α -GFP in excitatory presynaptic CFs can trans-synaptically recruit inhibitory GABA_ARs to postsynapses on PCs (**Figure 6F**).

Discussion

We have identified distinct presynaptic dependency of postsynaptic receptors at excitatory and inhibitory synapses in vivo. Specifically, we found that while excitatory AMPARs can localize to PSDs in the absence of presynaptic terminals, inhibitory GABA_ARs require inhibitory presynaptic components for postsynaptic clustering. Altogether, our findings reveal that fundamentally dissimilar machineries maintain different classes of postsynaptic receptors in the mature brain.

Cell-autonomous elimination of neurons

In this study, we utilized *Stxbp1* cKO mice as a powerful tool to eliminate neurons in a cell-autonomous manner (**Figure 1**). *Stxbp1* deletion in 5-HT neurons results in early postnatal lethality (**Dudok et al., 2011**). Consistent with this observation, we found neonatal or early postnatal lethality of *Stxbp1*^{fl/fl} mice with various Cre lines, including *Emx1-Cre*, *CaMKII-Cre*, *Nos1-Cre*, *Grm2-Cre*, *Grik4-Cre*, and *PV-Cre*. This lethality precluded the use of these mice in studies of mature synapses. Thus, we utilized injections of AAV carrying Cre recombinase to target-specific neuronal populations (**Figure 5**). By combining the *Stxbp1*^{fl/fl} mouse with the AAV approach, the elimination of specific neurons subtypes can be achieved to evaluate the roles of those neurons on synaptic maintenance, protein function, and behavior, as well as the specificity of Cre recombinase expression. Using this highly selective approach, the overall organization and integrity of the cerebellum remained remarkably intact (**Figure 1**), despite being reduced by >50% in size and the almost complete removal of specific cell populations. Thus, the brain's capacity to remove cell debris and maintain integrity of the remaining network likely copes with such massive cell loss without triggering generalized degenerative responses.

Machinery for stabilizing receptors at postsynaptic densities

Previous studies proposed that networks of cytosolic, transmembrane, and secreted proteins keep neurotransmitter receptors at postsynaptic sites (**Barrera-Ocampo and Chater, 2013; Gerrow and El-Husseini, 2007; Luscher et al., 2011; Martenson and Tomita, 2015; Moss and Smart, 2001**). Surprisingly, our results indicate that presynaptic terminals are required to retain postsynaptic GABA_ARs but not AMPARs (**Figures 2–5**), indicating that presynaptic protein, presumably a secreted or transmembrane protein(s), is required to maintain GABA_ARs at inhibitory synapses, whereas AMPARs require some postsynaptic protein(s), presumably, cytosolic or transmembrane protein(s), for maintenance at excitatory synapses, such as PSD-95-like MAGUK family proteins among others (**Garner et al., 2000; Kim and Sheng, 2004**). Also, presynaptic proteins, including Nrnx and Punctin/Madd-4, can induce or specify inhibitory synapses (**Graf et al., 2004; Maro et al., 2015; Pinan-Lucarré et al., 2014**), which is consistent with our finding that expression of Nrnx3 α by excitatory presynaptic neurons recruited GABA_ARs to postsynaptic sites (**Figure 6**). However, not all CF terminals expressing neurexin colocalized with GABA_ARs on PCs (**Figure 6**), and this appeared to be independent of the expression level of Nrnx3 α . This could be due to the lack of neurexin at the precise presynaptic

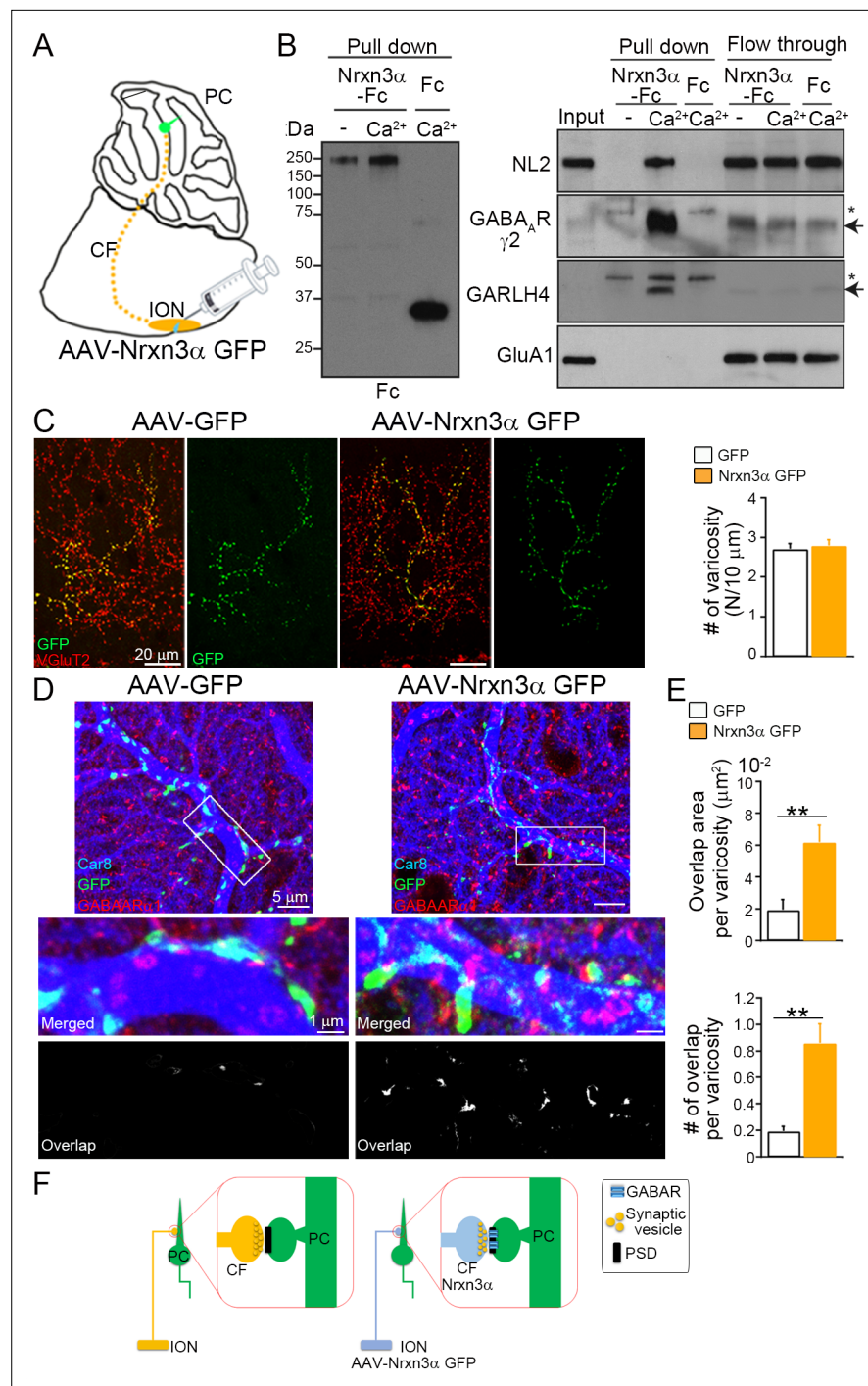


Figure 6. Ectopic Nrnx3 expression in excitatory climbing fibers (CFs) recruits inhibitory GABAergic receptors. (A) Adenoassociated viruses (AAVs) carrying GFP or Nrnx3α fused with GFP (Nrnx3α GFP) are injected into the inferior olivary nucleus (IONs) that project excitatory CFs to Purkinje cells (PCs). (B) The extracellular domain of neurexin-3 alpha (Nrnx3α) fused with Fc and secreted Fc are pulled down with protein A and used for pull down with adult mouse cerebellar lysate with and without calcium (Ca²⁺). Nrnx3α-Fc pulls down neuroligin 2 (NL2), GABA_ARγ2, and GARLH4, but not GluA1, in a calcium-dependent manner. The unbound proteins are detected in both conditions with and without calcium, suggesting no obvious protein degradation. Arrows and asterisks indicate specific and nonspecific bands, respectively. The raw images are provided in source data. (C) Both GFP and Nrnx3α-GFP (green) are colocalized with presynaptic VGLUT2 (red) along CF arbors. No significant difference is found between AAV-GFP and AAV-Nrxn3α-GFP in the number of GFP-positive varicosities per 10 μm axon of labeled CFs. Figure 6 continued on next page

Figure 6 continued

(N/10 μm) ($n = 34\text{--}50$ images from three GFP- and Nrnx3 α GFP-injected mice). (D, E) GABA $_A$ R clustering at CF–PC synapses is frequently detected after transfection of AAV-Nrnx3 α GFP, as shown by triple immunofluorescence for Car8 (blue), GFP (green), and GABA $_A$ R α 1 (red). (E) The area and number of overlapped regions between GFP and GABA $_A$ R α 1 per single CF varicosity ($n = 7\text{--}18$ images from three AAV-injected mice). (F) Nrnx3 α expression in excitatory CF induces clustering of inhibitory GABA $_A$ R α 1 at the CF–PC postsynapse. Data are shown as means \pm SEMs, Mann–Whitney *U*-test (D, E); ** $p < 0.01$. The numerical values are summarized in source data.

The online version of this article includes the following source data for figure 6:

Source data 1. Ectopic Nrnx3 expression in excitatory climbing fibers (CFs) recruits inhibitory GABA $_A$ R α 1.

nanodomain, as recent studies propose a relationship between the nanodomain structure of synapses and receptor localization (Biederer et al., 2017; Crosby et al., 2019). Future investigation is needed to characterize receptor and terminal organization in a more quantitative manner.

Excitatory presynaptic proteins have been proposed to be necessary for maintaining AMPARs at synapses (Barrera-Ocampo and Chater, 2013; Gerrow and El-Husseini, 2007; Martenson and Tomita, 2015), whereas we show that the presynaptic terminal is not required for maintaining AMPARs at the synapse (Figures 2 and 3). We propose three potential reasons for this discrepancy. (1) Changes in synaptogenesis or AMPAR maintenance at synapses. If proteins are involved in early synaptogenesis, net results from altered synaptogenesis may affect receptor maintenance at postsynaptic sites. In our study, we eliminated presynaptic neurons during or after synapse establishment (Figure 1 and Figure 1—figure supplement 1). (2) Poor resolution in the analysis of synapses. However, we utilized electron microscopy, a high-resolution cell biological approach, and uncaged glutamate responses at single dendritic spines to demonstrate no changes in excitatory receptor localization and function. Because presynaptic neurons were eliminated, we could not evaluate synaptic transmission. Thus, there could be a modest difference in postsynaptic localization of receptors, as a result of variability in image analyses. (3) Divergent mechanisms for maintenance of AMPARs at different type of synapses. However, we showed that trans- and postsynaptic mechanisms for maintenance of AMPARs are conserved between two different types of cerebellar synapses in vivo. Of note, demonstrating this mechanism at other excitatory synapse in the brain requires the complete removal of presynaptic or postsynaptic cell type, which is not easy to achieve in most brain areas.

Homo- and heterophilic machinery for maintaining synapses

We were able to eliminate excitatory inputs onto PCs and MLIs in vivo, and we observed two unusual types of structures in wild-type neurons, namely, free spines and dendrodendritic postsynaptic contacts, whereas the structure of spines and the PSD were maintained (Figures 2 and 3). PCs can generate and maintain spines without presynaptic terminals, but dynamic properties of PC spines might be different without presynapses. Remarkably, Cbln1 KO and GluD2 KO mice showed 80% and 60% of free spines, respectively (Hirai et al., 2005; Kurihara et al., 1997). It remains unclear why some spines are normal, and some spines lost presynaptic terminals. In addition, free spines have not been observed in different brain regions, for example, hippocampus (Yuste and Bonhoeffer, 2004), which may indicate that free spines are unstable in the hippocampus.

The elimination of PF input resulted in the formation of MLI dendrodendritic contact sites (Figure 3F). These contacts were unique in that AMPARs were localized at both sides of the contact, with the wider ‘cleft’ resembling an adhesive junction. It is possible that postsynaptic sites on MLI’s dendritic shafts express a protein that can form homophilic interactions, such as between cadherin and SynCAM proteins (Biederer et al., 2002; Gavilondo et al., 1982). Homophilic interactions may not occur in the presence of higher affinity pre- and postsynaptic protein interactions at normal synapses. In contrast, such homophilic interactions were rare for free spines on PCs in the Δ GC mice, suggesting differences in the molecular compositions of the PSD between PC spines and MLI dendrites or surrounded cell types. For example, after PFs were eliminated, the PSDs of PC spines may have been stabilized by Bergmann glia, specialized astrocytes in the cerebellum that enwrap PCs but not MLIs (Lemky-Johnston and Larramendi, 1968; Špaček, 1985). Future identification of molecules necessary to maintain pre- and postsynaptic sites may explain the difference Continued on next page in presynaptic-dependent morphology between spine and shaft synapses.

Materials and methods

Key resources table

Reagent type (species) or resource	Designation	Source or reference	Identifiers	Additional information
Strain, strain background (<i>Escherichia coli</i>)	Putative <i>Nos1</i> promoter	BACPAC Resources Center (BPRC)	BAC: RP24-84E3	
Strain, strain background (<i>Escherichia coli</i>)	Putative <i>Grin3a</i> promoter	BACPAC Resources Center (BPRC)	BAC: RP23-104D24	
Strain, strain background (<i>Escherichia coli</i>)	Putative <i>Kit</i> promoter	BACPAC Resources Center (BPRC)	BAC: RP23-232H18	
Strain, strain background (<i>Mus musculus</i>)	Wild-type (C57BL/6 J)	The Jackson Laboratory	Stock# 00064	
Strain, strain background (<i>Mus musculus</i>)	Mouse: <i>Stxbp1</i> ^{lox/lox}	Verhage et al., 2000	N/A	
Strain, strain background (<i>Mus musculus</i>)	Mouse: Tg(<i>Gabra6-Cre</i>)	MMRRC	ID# 015966-UCD	
Strain, strain background (<i>Mus musculus</i>)	Mouse: Tg(<i>Pcp2-Cre</i>)	The Jackson Laboratory	Stock# 004146	
Cell line (<i>Homo sapiens</i>)	293AAV	Cell Biolab	Cat#: AAV-100	
Antibody	anti- GABAAR α 1 (Rabbit polyclonal)	Frontier Inst.	Cat# GABAAR α 1-Rb-Af660 RRID:AB_2571571	IHC (1 μ g/ml)
Antibody	anti-GluD2 (Rabbit polyclonal)	Frontier Inst.	Cat# GluD2C-Rb-Af1200 RRID:AB_2571601	IHC (1 μ g/ml)
Antibody	anti-panAMPAR (Guinea pig polyclonal)	Frontier Inst.	Cat# panAMPAR-GP-Af580, RRID:AB_2571610	IHC (1 μ g/ml) IEM (5 μ g/ml)
Antibody	anti-VGluT1 (Guinea pig polyclonal)	Frontier Inst.	Cat# VGluT1-GP-Af570, RRID:AB_2571534	IHC (1 μ g/ml) IEM (10 μ g/ml)
Antibody	anti-VGluT2 (Guinea pig polyclonal)	Frontier Inst.	Cat# VGluT2-GP-Af810, RRID:AB_2341096	IHC (1 μ g/ml)
Antibody	anti-VIAAT (Guinea pig polyclonal)	Frontier Inst.	Cat# VGAT-GP-Af1000, RRID:AB_2571624	IHC (1 μ g/ml)
Antibody	anti-PSD95 (Guinea pig polyclonal)	Frontier Inst.	Cat# PSD95-GP-Af660, RRID:AB_2571539	IHC (1 μ g/ml)
Antibody	anti-GFP (Goat polyclonal)	Frontier Inst.	Cat# GFP-Go-Af1480, RRID:AB_2571574	IHC (1 μ g/ml)
Antibody	anti-calbindin (Goat polyclonal)	Frontier Inst.	Cat# Calbindin-Go-Af1040, RRID:AB_2532104	IHC (1 μ g/ml)
Antibody	anti-MAP2 (Goat polyclonal)	Frontier Inst.	Cat# MAP2-Go-Af860, RRID:AB_2571557	IHC (1 μ g/ml)
Antibody	anti-Car8 (Goat/Rabbit polyclonal)	Frontier Inst.	Cat# Car8-Go-Af780, RRID:AB_2571668 Cat# Car8-Rb-Af330, RRID:AB_2571667	IHC (1 μ g/ml) IEM (10 μ g/ml)
Antibody	anti-Bassoon (Mouse monoclonal)	Enzo	Cat# SAP7F407, RRID:AB_2313990	IHC (1 μ g/ml) IEM (20 μ g/ml)
Antibody	anti-GABAAR γ 2 (Rabbit polyclonal)	Millipore	Cat#: AB5559, RRID: AB_11211236	WB (1:2000)

Reagent type (species) or resource	Designation	Source or reference	Identifiers	Additional information
Antibody	anti-GARLH4 (Rabbit polyclonal)	<i>Yamasaki et al., 2017</i>	N/A	WB (0.1 µg/ml)
Antibody	anti-GluA1 (Rabbit polyclonal)	Millipore	Cat#: AB1504, RRID: AB_2113602	WB (1:2000)
Recombinant DNA reagent	pAAV-DJ (plasmid)	Cell Biolabs	VPK-410-DJ	
Recombinant DNA reagent	pHelper (plasmid)	Cell Biolabs	VPK-410-DJ	
Recombinant DNA reagent	pAAV-MCS (plasmid)	Cell Biolabs	VPK-410	
Recombinant DNA reagent	pAAV-Promoter less (plasmid)	This paper	N/A	pAAV-MCS (Cell Biolabs)
Recombinant DNA reagent	Nrxn3alpha pXY-Asc (plasmid)	Horizon	Cat# MMM1013-202798372	
Sequence-based reagent	B1.Nrxn3a.For	This paper	PCR primers	GGGGACAAG TTGTACAAAA AAGCAGGCTC CACCATGAG CTTTACCCT CCACTCAG TTTTCTTC
Sequence-based reagent	Nrxn3a(-).B5.Rev	This paper	PCR primers	GGGGACAAC TTGTATACAA AGTTGTACAT AATACTCCTTG TCCTTGTTTT CTGTTTC
Sequence-based reagent	B5.(-M)AcGFP.Fo	This paper	PCR primers	GGGGACAA CTTTGTATA CAAAAGTT GTGAGCAA GGGCGCC GAGCTGTTC
Sequence-based reagent	AcGFP*.B2.Rev	This paper	PCR primers	GGGGACCAC TTGTACAAGA AAGCTGGGT TCACTTGTTAC AGCTCATCCATGCC
Sequence-based reagent	AsCl.DEST.for	This paper	PCR primers	TACATGGCGC GCCACAAGTT TGTACAAAAAAGC
Sequence-based reagent	DEST.BsiWI.rev	This paper	PCR primers	ATGTACGTAC GACCACTTTG TACAAGAAAGC
Sequence-based reagent	B5.cre.For	This paper	PCR primers	GGGGACAAC TTGTATACAA AAGTTGCCACC ATGTCCAATTT ACTGACCG TACACC
Sequence-based reagent	cre*.B2.Rev	This paper	PCR primers	GGGGACCACT TTGTACAAGAA AGCTGGGTCA ATCGCCATCTT CCAGCAGGCG

Reagent type (species) or resource	Designation	Source or reference	Identifiers	Additional information
Sequence-based reagent	B1.pNOS.For	This paper	PCR primers	GGGGACAAGT TTGTACAAAA AGCAGGCTC CCCTCACCCAT CCCCACCCAC CTCCATCCATAC
Sequence-based reagent	pNOS.B5.Rev	This paper	PCR primers	GGGGACAA CTTTTGTAT ACAAAGTTGTT GCCGTTTCGGC CTTGGGTGG CATGATTC
Sequence-based reagent	B1.pGRIN3A.For	This paper	PCR primers	GGGGACAA GTTTGTACA AAAAAGCAG GCTCCCTGC CGTGCAAGGA CCACACATT CTACACTATAC
Sequence-based reagent	pGRIN3A.B5.Rev	This paper	PCR primers	GGGGACAACTT TTGTATACAAA GTTGTCGGCCA CCTTACCGCGG GCTCCCCCA GCGCCTGG
Sequence-based reagent	B1.pC-KIT.For	This paper	PCR primers	GGGGACAA GTTTGTACAAA AAAGCAGGCTG TCCACCCCG GATAGCCACAG TGACTGTGAAATG
Sequence-based reagent	pC-KIT.B5.Rev	This paper	PCR primers	GGGGACAA CTTTTGTAT ACAAAGTTGT GTGCACCGAG CGCGGCAAA GCCGAGC
Commercial assay or kit	Endofree QIAGEN Maxi kit	QIAGEN	QIAGEN Cat#12,362	
Chemical compound, drug	L-Glutamine	GIBCO	25030-081	
Chemical compound, drug	Penicillin– streptomycin	GIBCO	15140-122	
Chemical compound, drug	DMEM media	SIGMA	11965092	
Chemical compound, drug	Iscove's modified DM (IMDM)	Thermo	12440053	
Chemical compound, drug	Benzonase nuclease	Sigma	E1014-25kU	
Chemical compound, drug	Pfu Turbo DNA polymerase	Agilent	600,250	
Software, algorithm	MetaMorph	Molecular Devices	RRID:SCR_002368	

Animals

All animal handling was in accordance with protocols approved by the Institutional Animal Care and Use Committee (IACUC) of Yale University (Animal Welfare Assurance# D16-00146, Animal protocol number 2021-11029), the Albert Einstein College of Medicine (Animal Welfare Assurance# A3312-011, Animal protocol number 00001043) and Hokkaido University, Japan (Approval number, #19-0111). Animal care and housing were provided by the Yale Animal Resource Center (YARC), in

compliance with the Guide for the Care and Use of Laboratory Animals (National Academy Press, Washington, DC, 1996). Wild-type (C57BL/6 J, Stock# 000664), the transgenic Cre mouse under the *Pcp2* promoter (Barski et al., 2000) (Stock# 004146) were obtained from the Jackson Laboratory. The transgenic Cre mouse under the *Gabra6* promoter (Fünfschilling and Reichardt, 2002) (ID# 015966-UCD) was obtained from MMRRC. *Pcp2-Cre: Stxbp1^{fl/fl}* (Δ PC) mice exhibited mild ataxia and survived at least 6 months without extra care, whereas *Gabra6-Cre: Stxbp1^{fl/fl}* (Δ GC) mice were unable to stand, requiring food pellets and water to be supplied on the cage floor for survival.

Cell lines

293AAV cells were obtained directly from Cell Biolab, Inc and used them within 20 passages with continuous monitoring of cell morphology. Cells were grown at 37 °C, 5 % CO₂. The cell line was tested negative for mycoplasma contamination. The cell identity relies on Cell Biolabs (Cat#AAV-100).

Antibodies

The following antibodies were used at the indicated concentrations: rabbit polyclonal antibodies to GABAAR α 1 (rabbit, 1 μ g/ml for IHC (immunohistochemistry), Frontier Inst. GABAAR α 1-Rb-Af660, RRID:AB_2571571), GFP (goat, 1 μ g/ml for IHC, Frontier Inst. GFP-Go-Af1480, RRID:AB_2571574), panAMPA (guinea pig, 1 μ g/ml for IHC, 5 μ g/ml for ImmunoEM, Frontier Inst. panAMPA-GP-Af580, RRID:AB_2571610), GluD2 (rabbit, 1 μ g/ml for IHC, Frontier Inst. GluD2C-Rb-Af1200, RRID:AB_2571601), VGluT1 (guinea pig, 1 μ g/ml for IHC (Miyazaki et al., 2003), Frontier Inst. VGluT1-GP-Af570, RRID:AB_2571534), VGluT2 (guinea pig, 1 μ g/ml for IHC (Miyazaki et al., 2003), Frontier Inst. VGluT2-GP-Af810, RRID:AB_2341096), VIAAT (guinea pig, 1 μ g/ml for IHC (Miyazaki et al., 2003), Frontier Inst. VGAT-GP-Af1000, RRID:AB_2571624), PSD-95 (guinea pig, 1 μ g/ml for IHC, 10 μ g/ml for ImmunoEM (Fukaya and Watanabe, 2000), Frontier Inst. PSD95-GP-Af660, RRID:AB_2571539), calbindin (goat, 1 μ g/ml for IHC, Frontier Inst. Calbindin-Go-Af1040, RRID:AB_2532104), Car8 (goat, 1 μ g/ml for IHC; rabbit, 10 μ g/ml for ImmunoEM (Patrizi et al., 2008), Frontier Inst. Car8-Go-Af780, Car8-Rb-Af330, RRID:AB_2571667/2571668), MAP2 (goat, 1 μ g/ml for IHC, Frontier Inst. MAP2-Go-Af860, RRID:AB_2571557), Bassoon (mouse, 1 μ g/ml for IHC, 20 μ g/ml for ImmunoEM, Enzo, Cat# SAP7F407, RRID:AB_2313990), GABAAR γ 2 (rabbit, 1:2000 for immunoblot, Millipore. AB5559, RRID: AB_11211236), GARLH4 (rabbit, 0.1 μ g/ml for immunoblot, Yamasaki et al., 2017), and GluA1 (rabbit, 1:2000 for immunoblot, Millipore, AB1504, RRID:AB_2113602).

Immunostaining

Adult mice were deeply anesthetized with pentobarbital and perfused transcardially with 4 % paraformaldehyde in 0.1 M phosphate buffer (PB, pH 7.4). After postfixation for 3 hr, 50 μ m sections were prepared using a vibratome (Leica). In staining for postsynaptic molecules, sections were incubated with 1 mg/ml pepsin (Dako) in 0.2 N HCl at 37 °C for 2 min to facilitate antibody access to antigen molecules condensed in the postsynapse (Fukaya and Watanabe, 2000), stained with the appropriate primary and secondary antibodies and mounted with ProLong Gold (Thermo). Data were acquired using confocal microscopy (Zeiss LSM 800) with Plan-APOCHROMAT \times 63 oil immersion objective lens (Zeiss). Quantification analysis was performed using MetaMorph (Molecular Devices).

Virus production

AAV was prepared as described previously (McClure et al., 2011; Park et al., 2016). Briefly, three plasmids encoding the required components for AAV production were transfected into 293 AAV cells (Cell Biolab, Inc) using the calcium phosphate methods: AAV-DJ, pHelper (Cell Biolabs, Inc), and pAAV-CaM kinase II. For production of MLI-specific AAVs (pX), a putative promoter region of pAAV-synapsin vector was replaced into promoter region of *Nos-1*, *Grin3a*, *Kit* and obtained pX-GFP and pX-cre AAVs using with Gateway system (Thermo Fisher Scientific). After 48–60 hr post-transfection, cells were solubilized and AAVs were purified using a HiTrap Heparin column (GE healthcare).

Stereotaxic AAV injection

Under sterile conditions, 3–4 week-old animals were anesthetized with isoflurane and secured in a stereotaxic frame. For cerebellar injection, holes for injecting needles were drilled into the occipital bone and coordinates were (0, 0, and 1.0 mm; caudal to the occipital external protuberance, right to

midline, and ventral to pial surface, respectively) with tilting the manipulator at 50°. For injection into ION, the needle was inserted into the medulla, and injections were done unilaterally and coordinates (1.0, 1.5, and 1.8 mm; rostral to the rostral tip of the occipital bone, right to midline, and ventral to pial surface, respectively), with tilting the manipulator at 50 degrees. All injections were done with 1 µl of AAV per region. Mice were analyzed at 4 weeks after injection.

Electron microscopy

For conventional electron microscopy, mice were perfused transcardially with 2 % paraformaldehyde and 2 % glutaraldehyde in 0.1 M PB. The vibratome sections (400 µm in thickness) were immersed in 1 % OsO₄ for 15 min, dehydrated by graded alcohol and embedded into Epon812. After polymerization at 60 °C for 48 hr, ultrathin sections (~80 nm) were prepared by ultramicrotome (UCT, Leica).

For postembedding immunogold electron microscopy, mice were perfused transcardially with 4 % paraformaldehyde in 0.1 M PB. As described previously (Straub *et al.*, 2016), vibratome sections (400 µm in thickness) were cryoprotected with 30 % glycerol in PB, frozen rapidly with liquid propane in the EM CPC unit (Leica Microsystems), freeze-substituted to Lowicryl HM-20 resin (Electron Microscopy Sciences, Hatfield, PA), and polymerized with UV light by AFS unit (Leica). Ultrathin sections (~80 nm) on nickel grids were etched with saturation sodium-ethanolate solution for 1–5 s, and treated with following solutions: the donkey blocking solution containing 2 % normal donkey serum (Jackson ImmunoResearch) in Tris-buffered saline (TBS, pH 7.4) for 20 min, primary antibodies diluted with the donkey blocking solution overnight, and colloidal gold (10 nm)-conjugated species-specific IgG (1:100, British BioCell International, UK) in the donkey blocking solution for 2 hr. After extensive washing in TTBS and blocking with 2 % normal donkey serum, sections were further subjected to the second primary antibody and colloidal gold (15 nm)-conjugated species-specific secondary antibody. Sections were washed with TBS and distilled water, then stained with 1 % OsO₄ for 15 min, 2 % uranyl acetate for 4 min, and Reynold's lead citrate solution for 60 s. All electron microscopy images were taken with a JEM1400 electron microscope (JEOL, Japan). For quantitative analysis, postsynaptic membrane-associated immunogold particles, being defined as those apart <35 nm from the cell membrane, were counted on scanned electron micrographs and analyzed using MetaMorph software (Molecular Devices).

Pull down with Fc fusion proteins

Either the extracellular domain of mouse neurexin-3 alpha SS4+ (Horizon, MMM1013-202798372) or the signal peptide from GluA1 was fused with the human Fc domain and cloned into pcDNA3 expression vector (Invitrogen). HEK293T cells (ATCC, CRL-3216) were transfected with the plasmids using Lipofectamine 2000 according to the manufacturer's protocol. After 48 hr, the cultured media were collected and secreted Fc fusion proteins were purified with Protein A-sepharose (GE Healthcare). Mouse cerebella were solubilized with 25 mM Tris-Cl pH8.0, 1 % lauryl maltose neopentyl glycol (LMNG, Anatrace), Halt protease inhibitor (Thermo Fisher), and centrifuged at 100,000 × *g* for 30 min (Yamasaki *et al.*, 2017). Supernatants were then incubated with Fc fusion proteins on the protein A beads with 2 mM CaCl₂ and 2 mM MgCl₂ or with 5 mM EDTA. Beads were then washed six times with 0.1 % LMNG, 40 mM Tris-HCl pH 8.0 with or without 2 mM CaCl₂, 2 mM MgCl₂. Bound proteins were eluted by heating the resin in 1× SDS-PAGE sample buffer and analyzed by SDS-PAGE. Input lanes contained 5 % of the protein used for immunoprecipitation.

Two-photon imaging and MNI-glutamate uncaging

Acute sagittal cerebellar slices (250 µm thick) were prepared from adult control and ΔGC mice. Briefly, mice were anesthetized with isoflurane and euthanized by decapitation. Brains were removed and dissected using a VT1200S microslicer (Leica Microsystems Co.) in an ice-cold cutting solution containing (in mM): 110 choline, 2.5 KCl, 25 NaHCO₃, 1.25 NaH₂PO₄, 0.5 CaCl₂, 7 MgCl₂, 25 D-glucose, 11.6 sodium l-ascorbate, and 3.1 sodium pyruvate. Slices were then transferred and incubated for 15 min in a chamber placed in a warm bath (33–34°C) with oxygenated artificial cerebrospinal fluid (ACSF) solution containing (in mM): 124 NaCl, 2.5 KCl, 26 NaHCO₃, 1 NaH₂PO₄, 2.5 CaCl₂, 1.3 MgSO₄, and 10 D-glucose. Slices were then kept at room temperature for at least 30 min prior to recording. All solutions were equilibrated with 95 % O₂ and 5 % CO₂ (pH 7.4).

All electrophysiology and imaging experiments were performed at $32^{\circ}\text{C} \pm 1^{\circ}\text{C}$ in a submersion-type recording chamber perfused at 2 ml/min with ACSF supplemented with the GABA_A receptor antagonist picrotoxin (100 μM) and MNI-glutamate (2.5 mM). Whole-cell patch-clamp recordings using a Multiclamp 700 A amplifier (Molecular Devices) were made from PCs voltage clamped at -60 mV using patch-type pipette electrodes ($\sim 2\text{--}3$ M Ω) containing (in mM): 135 KMeSO₄, 5 KCl, 1 CaCl₂, 5 NaOH, 10 HEPES, 5 MgATP, 0.4 Na₃GTP, 5 EGTA, and 10 D-glucose, pH 7.2. The morphological indicator Alexa 594 (20 μM) was added to the pipette and allowed to diffuse and equilibrate for >30 min.

An Ultima 2 P microscope (Bruker Corp.) equipped with an Insight DeepSee laser and a MaiTai HP laser (Spectra Physics) was used for imaging and uncaging. Excitation wavelength for imaging and uncaging were 820 and 720 nm, respectively. Uncaging laser was parked ~ 1 μm far from the head of the target spine, and two uncaging pulses (1 ms duration, 100 Hz) were elicited. Electrophysiological data were acquired at 5 kHz, filtered at 2.4 kHz using IgorPro 7.01 (Wavemetrics, Inc). Statistical significance was assessed using OriginPro (OriginLaboratory).

Statistics

Quantification and statistical details of experiments can be found in the figure legends. All data are given as mean \pm SEM. The normality of distributions was assessed using the Shapiro–Wilk test. In data sets that were normally distributed, paired or unpaired Student's *t*-test and one-way analysis of variance with Bonferroni post hoc test were used to assess between-group differences. For the nonparametric tests, Mann–Whitney *U*-test and Kruskal–Wallis test followed by Steel or Steel–Dwass post-test. Statistical significance was set to $p < 0.05$, and statistically significant differences are indicated as follows: * $p < 0.05$, ** $p < 0.01$, and *** $p < 0.001$.

Acknowledgements

The authors thank Drs. Janghoo Lim, Pietro De Camilli, Shaul Yogev, and Marc Hammarlund for providing their valuable comments and the members of the Tomita lab for discussions. We thank Dr. Louis Reichardt for sharing transgenic Cre mice under the *Gabra6* promoter through the MMRRRC; Dr. Michael Meyer for sharing transgenic Cre mice under the *Pcp2* promoter through the Jackson Laboratory; and Addgene for the plasmids listed in Experimental Procedures.

Additional information

Competing interests

The authors declare that no competing interests exist.

Funding

Funder	Grant reference number	Author
NIH Office of the Director	MH115705	Susumu Tomita
NIH Office of the Director	MH077939	Susumu Tomita
Ministry of Education, Culture, Sports, Science and Technology	Grant-in-Aid for Scientific Research 17K08485	Taisuke Miyazaki
Ministry of Education, Culture, Sports, Science and Technology	Grant-in-Aid for Scientific Research 18K06813	Taisuke Miyazaki
NIH Office of the Director	F32NS093952	Yoav Noam
NIH Office of the Director	NS113600	Pablo E Castillo
NIH Office of the Director	MH125772	Pablo E Castillo

Funder **Grant reference number** **Author**

The funders had no role in study design, data collection and interpretation, or the decision to submit the work for publication.

Author contributions

Taisuke Miyazaki, Data curation, Formal analysis, Investigation, Methodology, Project administration, Validation, Visualization, Writing - original draft, Writing - review and editing; Megumi Morimoto-Tomita, Investigation, Methodology, Resources, Validation, Writing - review and editing; Coralie Berthoux, Formal analysis, Methodology, Writing - review and editing; Kotaro Konno, Investigation, Validation, Writing - review and editing; Yoav Noam, Data curation, Investigation, Methodology, Validation, Writing - review and editing; Tokiwa Yamasaki, Methodology, Writing - review and editing; Matthijs Verhage, Resources, Writing - review and editing; Pablo E Castillo, Data curation, Funding acquisition, Supervision, Writing - review and editing; Masahiko Watanabe, Data curation, Methodology, Supervision, Writing - review and editing; Susumu Tomita, Conceptualization, Data curation, Funding acquisition, Investigation, Methodology, Project administration, Resources, Supervision, Visualization, Writing - original draft, Writing - review and editing

Author ORCIDs

Pablo E Castillo  <http://orcid.org/0000-0002-9834-1801>

Masahiko Watanabe  <http://orcid.org/0000-0001-5037-7138>

Susumu Tomita  <http://orcid.org/0000-0001-8344-259X>

Ethics

All animal handling was in accordance with protocols approved by the Institutional Animal Care and Use Committee (IACUC) of Yale University (Animal Welfare Assurance# D16-00146, Animal protocol number 2021-11029), the Albert Einstein College of Medicine (Animal Welfare Assurance# A3312-011, Animal protocol number 00001043), and Hokkaido University, Japan (Approval number, #19-0111). Animal care and housing were provided by the Yale Animal Resource Center (YARC), in compliance with the Guide for the Care and Use of Laboratory Animals (National Academy Press, Washington, DC, 1996).

Decision letter and Author response

Decision letter <https://doi.org/10.7554/eLife.59613.sa1>

Author response <https://doi.org/10.7554/eLife.59613.sa2>

Additional files**Supplementary files**

- Transparent reporting form

Data availability

All data generated or analyzed during this study are included in the manuscript and supporting file. Source Data files showing all raw values for each figure and the original images of uncropped blots for Figure 6B have been provided.

References

- Altman J, Anderson WJ. 1972. Experimental reorganization of the cerebellar cortex. I. Morphological effects of elimination of all microneurons with prolonged x-irradiation started at birth. *The Journal of Comparative Neurology* **146**: 355–406. DOI: <https://doi.org/10.1002/cne.901460305>, PMID: 5086676
- Aoto J, Földy C, Ilcus SMC, Tabuchi K, Südhof TC. 2015. Distinct circuit-dependent functions of presynaptic neurexin-3 at GABAergic and glutamatergic synapses. *Nature Neuroscience* **18**: 997–1007. DOI: <https://doi.org/10.1038/nn.4037>, PMID: 26030848
- Barrera-Ocampo A, Chater TE. 2013. Contribution of postsynaptic molecules to AMPA receptor nanodomain organization. *The Journal of Neuroscience* **33**: 19048–19050. DOI: <https://doi.org/10.1523/JNEUROSCI.4273-13.2013>, PMID: 24305802
- Barski JJ, Dethleffsen K, Meyer M. 2000. Cre recombinase expression in cerebellar Purkinje cells. *Genesis* **28**: 93–98. DOI: [https://doi.org/10.1002/1526-968X\(200011/12\)28:3/4<93::AID-GENE10>3.0.CO;2-W](https://doi.org/10.1002/1526-968X(200011/12)28:3/4<93::AID-GENE10>3.0.CO;2-W), PMID: 11105049

- Bayer SA**, Altman J. 1975. The effects of X-irradiation on the postnatally-forming granule cell populations in the olfactory bulb, hippocampus, and cerebellum of the rat. *Experimental Neurology* **48**: 167–174. DOI: [https://doi.org/10.1016/0014-4886\(75\)90231-9](https://doi.org/10.1016/0014-4886(75)90231-9), PMID: 1132466
- Biederer T**, Sara Y, Mozhayeva M, Atasoy D, Liu X, Kavalali ET, Südhof TC. 2002. SynCAM, a synaptic adhesion molecule that drives synapse assembly. *Science* **297**: 1525–1531. DOI: <https://doi.org/10.1126/science.1072356>, PMID: 12202822
- Biederer T**, Kaeser PS, Blanpied TA. 2017. Transcellular Nanoalignment of Synaptic Function. *Neuron* **96**: 680–696. DOI: <https://doi.org/10.1016/j.neuron.2017.10.006>, PMID: 29096080
- Chen LY**, Jiang M, Zhang B, Gokce O, Südhof TC. 2017. Conditional Deletion of All Neurexins Defines Diversity of Essential Synaptic Organizer Functions for Neurexins. *Neuron* **94**: 611–625. DOI: <https://doi.org/10.1016/j.neuron.2017.04.011>, PMID: 28472659
- Craig AM**, Kang Y. 2007. Neurexin-neuroigin signaling in synapse development. *Current Opinion in Neurobiology* **17**: 43–52. DOI: <https://doi.org/10.1016/j.conb.2007.01.011>, PMID: 17275284
- Crosby KC**, Gookin SE, Garcia JD, Hahn KM, Dell'Acqua ML, Smith KR. 2019. Nanoscale Subsynaptic Domains Underlie the Organization of the Inhibitory Synapse. *Cell Reports* **26**: 3284–3297. DOI: <https://doi.org/10.1016/j.celrep.2019.02.070>, PMID: 30893601
- Davenport EC**, Pendolino V, Kontou G, McGee TP, Sheehan DF, López-Doménech G, Farrant M, Kittler JT. 2017. An Essential Role for the Tetraspanin LHFPL4 in the Cell-Type-Specific Targeting and Clustering of Synaptic GABAA Receptors. *Cell Reports* **21**: 70–83. DOI: <https://doi.org/10.1016/j.celrep.2017.09.025>, PMID: 28978485
- Dean C**, Dresbach T. 2006. Neuroligins and neurexins: linking cell adhesion, synapse formation and cognitive function. *Trends in Neurosciences* **29**: 21–29. DOI: <https://doi.org/10.1016/j.tins.2005.11.003>, PMID: 16337696
- Dudok JJ**, Groffen AJA, Toonen RFT, Verhage M. 2011. Deletion of Munc18-1 in 5-HT neurons results in rapid degeneration of the 5-HT system and early postnatal lethality. *PLOS ONE* **6**: e28137. DOI: <https://doi.org/10.1371/journal.pone.0028137>, PMID: 22140524
- Fritschy J-M**, Panzanelli P, Kralic JE, Vogt KE, Sassoè-Pognetto M. 2006. Differential dependence of axo-dendritic and axo-somatic GABAergic synapses on GABAA receptors containing the alpha1 subunit in Purkinje cells. *The Journal of Neuroscience* **26**: 3245–3255. DOI: <https://doi.org/10.1523/JNEUROSCI.5118-05.2006>, PMID: 16554475
- Fukaya M**, Watanabe M. 2000. Improved immunohistochemical detection of postsynaptically located PSD-95/SAP90 protein family by protease section pretreatment: a study in the adult mouse brain. *The Journal of Comparative Neurology* **426**: 572–586. DOI: [https://doi.org/10.1002/1096-9861\(20001030\)426:4<572::AID-CNE6>3.0.CO;2-9](https://doi.org/10.1002/1096-9861(20001030)426:4<572::AID-CNE6>3.0.CO;2-9), PMID: 11027400
- Fünfschilling U**, Reichardt LF. 2002. Cre-mediated recombination in rhombic lip derivatives. *Genesis* **33**: 160–169. DOI: <https://doi.org/10.1002/gene.10104>, PMID: 12203913
- Garner CC**, Nash J, Hagan RL. 2000. PDZ domains in synapse assembly and signalling. *Trends in Cell Biology* **10**: 274–280. DOI: [https://doi.org/10.1016/s0962-8924\(00\)01783-9](https://doi.org/10.1016/s0962-8924(00)01783-9), PMID: 10856930
- Gavilondo J**, Fernandez A, Castillo R, Lage A. 1982. Neoplastic progression evidenced in the L929 cell system. I. Selection of tumorigenic and metastasizing cell variants. *Neoplasia* **29**: 269–279. PMID: 7133224.
- Gerrow K**, El-Husseini A. 2007. Receptors look outward: revealing signals that bring excitation to synapses. *Science's STKE* **2007**: e56. DOI: <https://doi.org/10.1126/stke.4082007pe56>, PMID: 17940274
- Graf ER**, Zhang X, Jin SX, Linhoff MW, Craig AM. 2004. Neurexins induce differentiation of GABA and glutamate postsynaptic specializations via neuroligins. *Cell* **119**: 1013–1026. DOI: <https://doi.org/10.1016/j.cell.2004.11.035>, PMID: 15620359
- Gray DC**, Mahrus S, Wells JA. 2010. Activation of specific apoptotic caspases with an engineered small-molecule-activated protease. *Cell* **142**: 637–646. DOI: <https://doi.org/10.1016/j.cell.2010.07.014>, PMID: 20723762
- Hamodeh S**, Eicke D, Napper RMA, Harvey RJ, Sultan F. 2010. Population based quantification of dendrites: evidence for the lack of microtubule-associate protein 2a,b in Purkinje cell spiny dendrites. *Neuroscience* **170**: 1004–1014. DOI: <https://doi.org/10.1016/j.neuroscience.2010.08.021>, PMID: 20727947
- Hartzell HC**, Fambrough DM. 1972. Acetylcholine receptors. Distribution and extrajunctional density in rat diaphragm after denervation correlated with acetylcholine sensitivity. *The Journal of General Physiology* **60**: 248–262. DOI: <https://doi.org/10.1085/jgp.60.3.248>, PMID: 5055788
- Heeroma JH**, Roelandse M, Wierda K, van Aerde KI, Toonen RFG, Hensbroek RA, Brussaard A, Matus A, Verhage M. 2004. Trophic support delays but does not prevent cell-intrinsic degeneration of neurons deficient for munc18-1. *The European Journal of Neuroscience* **20**: 623–634. DOI: <https://doi.org/10.1111/j.1460-9568.2004.03503.x>, PMID: 15255974
- Hirai H**, Pang Z, Bao D, Miyazaki T, Li L, Miura E, Parris J, Rong Y, Watanabe M, Yuzaki M, Morgan JI. 2005. Cbln1 is essential for synaptic integrity and plasticity in the cerebellum. *Nature Neuroscience* **8**: 1534–1541. DOI: <https://doi.org/10.1038/nn1576>, PMID: 16234806
- Kim E**, Sheng M. 2004. PDZ domain proteins of synapses. *Nature Reviews. Neuroscience* **5**: 771–781. DOI: <https://doi.org/10.1038/nrn1517>, PMID: 15378037
- Kurihara H**, Hashimoto K, Kano M, Takayama C, Sakimura K, Mishina M, Inoue Y, Watanabe M. 1997. Impaired parallel fiber->Purkinje cell synapse stabilization during cerebellar development of mutant mice lacking the glutamate receptor delta2 subunit. *The Journal of Neuroscience* **17**: 9613–9623. PMID: 9391016.

- Landsend AS**, Amiry-Moghaddam M, Matsubara A, Bergersen L, Usami S, Wenthold RJ, Ottersen OP. 1997. Differential localization of delta glutamate receptors in the rat cerebellum: coexpression with AMPA receptors in parallel fiber-spine synapses and absence from climbing fiber-spine synapses. *The Journal of Neuroscience* **17**: 834–842 PMID: 8987804, DOI: <https://doi.org/10.1002/cne.901340105>, PMID: 5712412
- Lemkey-Johnston N**, Larramendi LM. 1968. Morphological characteristics of mouse stellate and basket cells and their neuroglial envelope: an electron microscopic study. *The Journal of Comparative Neurology* **134**: 39–72. DOI: <https://doi.org/10.1002/cne.901340105>, PMID: 5712412
- Luscher B**, Fuchs T, Kilpatrick CL. 2011. GABAA receptor trafficking-mediated plasticity of inhibitory synapses. *Neuron* **70**: 385–409. DOI: <https://doi.org/10.1016/j.neuron.2011.03.024>, PMID: 21555068
- Maro GS**, Gao S, Olechwiec AM, Hung WL, Liu M, Özkan E, Zhen M, Shen K. 2015. MADD-4/Punctin and Neurexin Organize C. elegans GABAergic Postsynapses through Neuroligin. *Neuron* **86**: 1420–1432. DOI: <https://doi.org/10.1016/j.neuron.2015.05.015>, PMID: 26028574
- Martenson JS**, Tomita S. 2015. Synaptic localization of neurotransmitter receptors: comparing mechanisms for AMPA and GABAA receptors. *Current Opinion in Pharmacology* **20**: 102–108. DOI: <https://doi.org/10.1016/j.coph.2014.11.011>, PMID: 25529200
- McClure C**, Cole KLH, Wulff P, Klugmann M, Murray AJ. 2011. Production and titrating of recombinant adeno-associated viral vectors. *Journal of Visualized Experiments* **1**: e3348. DOI: <https://doi.org/10.3791/3348>
- Miyazaki T**, Fukaya M, Shimizu H, Watanabe M. 2003. Subtype switching of vesicular glutamate transporters at parallel fibre-Purkinje cell synapses in developing mouse cerebellum. *The European Journal of Neuroscience* **17**: 2563–2572. DOI: <https://doi.org/10.1046/j.1460-9568.2003.02698.x>, PMID: 12823463
- Moss SJ**, Smart TG. 2001. Constructing inhibitory synapses. *Nature Reviews. Neuroscience* **2**: 240–250. DOI: <https://doi.org/10.1038/35067500>, PMID: 11283747
- Napper RM**, Harvey RJ. 1988. Number of parallel fiber synapses on an individual Purkinje cell in the cerebellum of the rat. *The Journal of Comparative Neurology* **274**: 168–177. DOI: <https://doi.org/10.1002/cne.902740204>, PMID: 3209740
- Palmiter RD**, Behringer RR, Quaife CJ, Maxwell F, Maxwell IH, Brinster RL. 1987. Cell lineage ablation in transgenic mice by cell-specific expression of a toxin gene. *Cell* **50**: 435–443. DOI: [https://doi.org/10.1016/0092-8674\(87\)90497-1](https://doi.org/10.1016/0092-8674(87)90497-1), PMID: 3649277
- Park J**, Chávez AE, Mineur YS, Morimoto-Tomita M, Lutz S, Kim KS, Picciotto MR, Castillo PE, Tomita S. 2016. CaMKII Phosphorylation of TARPγ-8 Is a Mediator of LTP and Learning and Memory. *Neuron* **92**: 75–83. DOI: <https://doi.org/10.1016/j.neuron.2016.09.002>, PMID: 27667007
- Patrizi A**, Scelfo B, Viltono L, Briatore F, Fukaya M, Watanabe M, Strata P, Varoqueaux F, Brose N, Fritschy J-M, Sassoè-Pognetto M. 2008. Synapse formation and clustering of neuroligin-2 in the absence of GABAA receptors. *PNAS* **105**: 13151–13156. DOI: <https://doi.org/10.1073/pnas.0802390105>, PMID: 18723687
- Pinan-Lucarré B**, Tu H, Pierron M, Cruceyra PI, Zhan H, Stigloher C, Richmond JE, Bessereau J-L. 2014. C. elegans Punctin specifies cholinergic versus GABAergic identity of postsynaptic domains. *Nature* **511**: 466–470. DOI: <https://doi.org/10.1038/nature13313>, PMID: 24896188
- Roth A**, Häusser M. 2001. Compartmental models of rat cerebellar Purkinje cells based on simultaneous somatic and dendritic patch-clamp recordings. *The Journal of Physiology* **535**: 445–472. DOI: <https://doi.org/10.1111/j.1469-7793.2001.00445.x>, PMID: 11533136
- Špaček J**. 1985. Three-dimensional analysis of dendritic spines. *Anatomy and Embryology* **171**: 245–252. DOI: <https://doi.org/10.1007/BF00341419>
- Straub C**, Noam Y, Nomura T, Yamasaki M, Yan D, Fernandes HB, Zhang P, Howe JR, Watanabe M, Contractor A, Tomita S. 2016. Distinct Subunit Domains Govern Synaptic Stability and Specificity of the Kainate Receptor. *Cell Reports* **16**: 531–544. DOI: <https://doi.org/10.1016/j.celrep.2016.05.093>, PMID: 27346345
- Südhof TC**. 2008. Neuroligins and neurexins link synaptic function to cognitive disease. *Nature* **455**: 903–911. DOI: <https://doi.org/10.1038/nature07456>, PMID: 18923512
- Uusisaari M**, Knöpfel T. 2011. Functional classification of neurons in the mouse lateral cerebellar nuclei. *Cerebellum* **10**: 637–646. DOI: <https://doi.org/10.1007/s12311-010-0240-3>, PMID: 21116763
- Verhage M**, Maia AS, Plomp JJ, Brussaard AB, Heeroma JH, Vermeer H, Toonen RF, Hammer RE, van den Berg TK, Missler M, Geuze HJ, Südhof TC. 2000. Synaptic assembly of the brain in the absence of neurotransmitter secretion. *Science* **287**: 864–869. DOI: <https://doi.org/10.1126/science.287.5454.864>, PMID: 10657302
- Watanabe D**, Inokawa H, Hashimoto K, Suzuki N, Kano M, Shigemoto R, Hirano T, Toyama K, Kaneko S, Yokoi M, Moriyoshi K, Suzuki M, Kobayashi K, Nagatsu T, Kreitman RJ, Pastan I, Nakanishi S. 1998. Ablation of cerebellar Golgi cells disrupts synaptic integration involving GABA inhibition and NMDA receptor activation in motor coordination. *Cell* **95**: 17–27. DOI: [https://doi.org/10.1016/s0092-8674\(00\)81779-1](https://doi.org/10.1016/s0092-8674(00)81779-1), PMID: 9778244
- Wu M**, Tian HL, Liu X, Lai JHC, Du S, Xia J. 2018. Impairment of Inhibitory Synapse Formation and Motor Behavior in Mice Lacking the NL2 Binding Partner LHFPL4/GARLH4. *Cell Reports* **23**: 1691–1705. DOI: <https://doi.org/10.1016/j.celrep.2018.04.015>, PMID: 29742426
- Yamasaki T**, Hoyos-Ramirez E, Martenson JS, Morimoto-Tomita M, Tomita S. 2017. GARLH Family Proteins Stabilize GABAA Receptors at Synapses. *Neuron* **93**: 1138–1152. DOI: <https://doi.org/10.1016/j.neuron.2017.02.023>, PMID: 28279354

- Yang CF**, Chiang MC, Gray DC, Prabhakaran M, Alvarado M, Juntti SA, Unger EK, Wells JA, Shah NM. 2013. Sexually dimorphic neurons in the ventromedial hypothalamus govern mating in both sexes and aggression in males. *Cell* **153**: 896–909. DOI: <https://doi.org/10.1016/j.cell.2013.04.017>, PMID: 23663785
- Yuste R**, Bonhoeffer T. 2004. Genesis of dendritic spines: insights from ultrastructural and imaging studies. *Nature Reviews. Neuroscience* **5**: 24–34. DOI: <https://doi.org/10.1038/nrn1300>, PMID: 14708001
- Zhang C**, Atasoy D, Araç D, Yang X, Fucillo MV, Robison AJ, Ko J, Brunger AT, Südhof TC. 2010. Neurexins physically and functionally interact with GABA(A) receptors. *Neuron* **66**: 403–416. DOI: <https://doi.org/10.1016/j.neuron.2010.04.008>, PMID: 20471353